Atlas Journal of Materials Science 2 (1): 44–47, 2015
doi: 10.5147/ajms.2015.0163

The Influence of Annealing Temperature on Microstructure and Magnetic Properties of $Fe_{74}Co_3Si_8B_{10}Al_1Nb_4$ Amorphous Alloy Ribbons

Shih Fan Chen[1*], Chih Yuan Chen[2*], and Chien Fan Chiang[1]

[1] Institute of Materials Science and Engineering, National Taipei University of Technology, Taipei 106, Taiwan;
[2] Department of Energy Engineering, National United University, Miaoli 36003, Taiwan

Received: January 10, 2015 / Accepted: February 27, 2015

Abstract

Multi-component alloy ribbons with a composition of $Fe_{74}Co_3Si_8B_{10}Al_1Nb_4$ were prepared by a single roller melt-spinning method. The alloy had a fully amorphous structure, as determined by X-ray diffraction. The alloy ribbons were annealed for 10 min at temperatures of 350, 400, 450, 500, 550 and 600 °C, respectively. Differential scanning calorimetry curves indicated that the glass transition temperature (T_g) and the supercooled liquid range (ΔT_x) of the amorphous alloy ribbon were about 494 °C and 43 °C, respectively. The ribbons showed soft magnetic properties, with a Curie temperature (T_c) at 284 °C, high saturation magnetization (M_s) of 1.18 T, and coercive force (Hc) of 33.66 A/m. In the present study, both saturation magnetization and coercive force of amorphous alloy ribbons increased with increasing the annealing temperature, due to precipitations and growth of α–Fe phase nanocrystals in the amorphous matrix. On the other hand, it was found that the coercive force of alloy ribbons reduced as a consequence of precipitations of Nb_3Si phase if the annealing temperature reached 600 °C.

Keywords: Annealing; Fe-base amorphous alloy; Magnetic property; Nanocrystals; Ribbon.

* Corresponding authors: sfchen@ntut.edu.tw; chen6563@gmail.com

Introduction

As compared with other bulk metallic glasses (BMGs), iron-based alloys are the most promising and attractive candidates for applications in the soft magnetic areas. Among many iron-based alloy glasses, $Fe_{73.5}Si_{13.5}B_9Cu_1Nb_3$ alloy (FINEMET) showed superior soft magnetic properties, with low coercive force (0.5~1 A/m) and high saturation magnetization which was greater than 1.2 T (Yoshizawa et al., 1988). The excellent magnetic properties of FINEMET alloy originated from its composite and structure, because the amorphous FINEMET alloy obtained after melt-spinning required further heat treatment (between 500 to 600 °C) to induce the precipitations of Fe-Si nanocrystals. Therefore the final nanostructured composites consisted of ferromagnetic nanograins embedded in a ferromagnetic amorphous matrix. Furthermore, the heat treatment of the alloy ribbons must be performed in the final toroid shape, since it becomes extremely brittle in the composite with nanocrystalline structure (Borrego et al, 2014; Chen et al., 2014; Wang et al., 2013; Zuo et al., 2005).

Although FINEMET has very good magnetic properties, its mechanical properties are still inferior to those of Fe-Co-B-Si-Nb alloys, because its constituent elements of the Fe-Co-B-Si-Nb alloy have strong chemical bonds (Inoue et al., 2004). On the other hand, it is believed that adding Al can effectively decrease the coercive force in nanocrystalline alloys (Mınguez et al., 2001). Therefore, it would be of interest to examine the magnetic properties of Fe-Co-B-Si-Nb-Al amorphous alloy after annealing at various temperatures.

In the present study, we focus on the annealing temperature dependence of microstructure and magnetic properties of $Fe_{74}Co_3Si_8B_{10}Al_1Nb_4$ amorphous material composed of a nanocrystalline phase in an amorphous matrix. Such dependence is very important in gaining insights into the nature of the magnetic properties of the material.

Experimental Procedure

Multi-component alloy ingots of $Fe_{74}Co_3Si_8B_{10}Al_1Nb_4$ were prepared by arc melting industrially pure Fe (99.5 wt.% purity), Co (99.5 wt.% purity), Si (99.9 wt.% purity), B (99.8 wt.% purity), Al (99.5 wt.% purity), and Nb (99.5 wt.% purity) under argon atmosphere. The alloys were then melted using a vacuum induction melting furnace, and the melt was injected onto a 200 mm diameter copper wheel rotating at 5000 rpm to form rapidly solidified ribbon specimens with 3~5 mm in width and 15~30 μm in thickness. All alloy ribbons were then annealed in vacuum for 10 min at 350, 400, 450, 500, 550, and 600 °C, respectively. X-ray diffraction (XRD, Rigaku DMX-2200VK/PC) with Cu K_α radiation operated at 40 kV was utilized to determine whether amorphous, glassy, or crystallized structures were formed. The glass transition temperature (T_g), crystallization temperature (T_x), and Curie temperature (T_c) of the as-quenched ribbons were measured using a differential scanning calorimeter (DSC, SDT-Q600 Simultaneous TGA/DSC) and a thermomagnetic analysis instrument (TMA, Perkin Elmer/TAC 7/DX) under an applied 110 Oe field, both at 0.667 °C/s. Finally, magnetic properties were examined by a vibrating sample magnetometer (VSM, DMS 1660) in an applied magnetic field up to 5,000 Oe.

Results and Discussion

The X-ray diffraction pattern of as-quenched $Fe_{74}Co_3Si_8B_{10}Al_1Nb_4$ alloy ribbon is presented in Fig. 1 (bottom side). The pattern shows only broad scattering at low angles and contains no sharp peaks, indicating that the amorphous phase of $Fe_{74}Co_3Si_8B_{10}Al_1Nb_4$ alloy ribbon was produced by the single roller melt-spinning method.

The characteristic temperatures of $Fe_{74}Co_3Si_8B_{10}Al_1Nb_4$alloy ribbon are summarized in Table 1. The T_g, T_x, and supercooled liquid region ($\Delta T_x = T_x - T_g$) of the amorphous alloy ribbon were 494, 537 and 43 °C, respectively. It is well known that the atomic clusters that initially precipitate in the amorphous matrix need to overcome their energy barrier. Since obtaining tiny crystal grains in the amorphous matrix with a larger energy barrier is very difficult, a large supercooled liquid region is needed for the overall crystallization process to be activated. In order to understand the effects of alloying elements on the stability of the melt against crystallization during cooling, we estimate the crystallization energy barrier of the $Fe_{74}Co_3Si_8B_{10}Al_1Nb_4$ alloy by the Kissinger equation as follows:

$$\ln[\beta/T_p^2] = E/R \times 1/T_p + \text{Constant} \qquad (1)$$

where E is crystallization energy barrier (kJ/mole), β is heating rate (K/min), Tp is crystallization peak temperature (K), and R is universal gas constant (J/mol K). Taking 3 different heating rates at 10, 15 and 20 °C/min, we can calculate 3 corresponding different peak crystallization temperatures, namely 544.76, 549.76 and 552.37 °C, respectively. Based on the above data, the crystallization energy barrier of the $Fe_{74}Co_3Si_8B_{10}Al_1Nb_4$ alloy is about 490 kJ/mole. As compared with the other values for crystallization energy barriers in Table 1 (Zhang et al., 2006; Ahmadi et al., 2010), the energy barrier for the $Fe_{74}Co_3Si_8B_{10}Al_1Nb_4$ alloy system is relatively high. It has been pointed out that a high ability of supercooled liquid to form amorphous phase can be obtained in alloy systems that satisfy Inoue's three empirical rules, which include (1) multi-component consisting of more than three elements, (2) significant atomic size mismatches above 12% among the main three elements, and (3) negative heats of mixing among the main elements (Inoue et al., 2000). The $Fe_{74}Co_3Si_8B_{10}Al_1Nb_4$ alloy system obeys Inoue's first requirement because of the constituent six elements. The atomic size ratios are 0.8 for Co/Fe and 6.8 to 38.9 for Co/(B, Si), 15.3 for Nb/Fe or Al/Fe, and 22.2 to 58.9 for Nb/(B, Si) or Al/(B, Si). In addition, the heat of mixing is -1 KJ/mol for Fe-Co pairs, -38 KJ/mol for Si-Co pairs, -24 KJ/mol for B-Co pairs, -16 KJ/mol for Fe-Nb pairs, -56 KJ/mol for Si-Nb pairs, -54 KJ/mol for B-Nb pairs, -11 KJ/mol for Fe-Al pairs, -19 KJ/mol for Si-Al pairs, and 0 KJ/mol for B-Al pairs [(akeuchi et al., 2005). Since the alloy satisfies the three empirical requirements, the present amorphous $Fe_{74}Co_3Si_8B_{10}Al_1Nb_4$ alloy system can achieve superior thermal stability.

Fig. 1 presents the variations in X-ray diffraction patterns of $Fe_{74}Co_3Si_8B_{10}Al_1Nb_4$ alloy annealed for 10 min at various temperatures. It can be seen that all samples annealed at temperatures below 500 °C exhibited broad scattering. On the other hand, specific diffraction peaks representing precipitations of α–Fe phase appear when the annealing temperature exceeded 500 °C, and these peaks become stronger as the annealing temperature rises up. The grain size of the α–Fe phase, measured by Debye-Scherrer method (Cullity, 2001), increase from 10.1 nm to 26.2 nm when the annealing temperature increases from 500 to 600 °C. In addition, FeB and Nb3Si also precipitate when the annealing temperature reaches to 600 °C.

Fig. 2 presents SEM micrographs of amorphous $Fe_{74}Co_3Si_8B_{10}Al_1Nb_4$ alloy annealed at different temperatures for 10 min. When the annealing temperature is 450 °C, the resulting morphology is dendritic. If the annealing temperature is higher

Table 1. Characteristic temperatures and crystallization energy barrier of Fe74Co3Si8B10Al1Nb4 and other alloys.

Alloy	Activation Energy (KJ/Mol)	T_g (°C)	T_x (°C)	ΔT_x (°C)	T_m (°C)	T_l (°C)
$Fe_{74}Co_3Si_8B_{10}Al_1Nb_4$	490	494	537	43	1051	1059
$Fe_{77.5}Co_{13.5}B_9$	376					
$Fe_{77.5}Co_{13.5}B_9Nb_3$	421					
$Fe_{76.5}Co_{13.5}B_9Cu_1$	236					
$Fe_{76.5}Co_{13.5}B_9Cu_1Nb_3$	301					
$Fe_{55}Cr_{18}Mo_7B_{16}C_4$	.276					

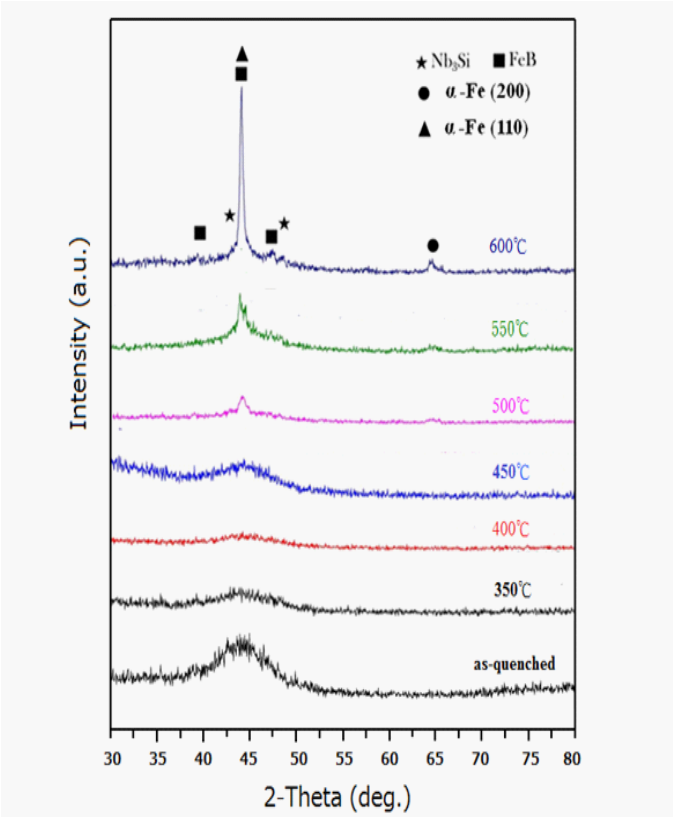

Figure 1. X-ray diffraction patterns of $Fe_{74}Co_3Si_8B_{10}Al_1Nb_4$ alloy ribbons annealed at various temperatures for 10 min. Alloy ribbons annealed below 450 °C composed of amorphous phase. Annealing above 500 °C results ferrite crystals precipitated in the amorphous matrix. FeB and Nb3Si phases are found in the alloy ribbon when annealing temperature reaches 600 °C.

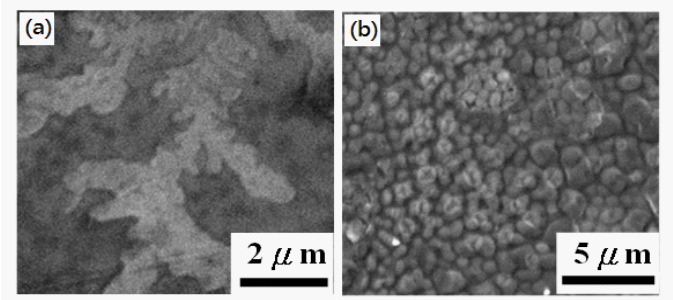

Figure 2. SEM micrographs of the Fe74Co3Si8B10Al1Nb4 alloy ribbons annealed at 450 °C (a) and 550 °C (b) for 10 minutes.

(~550 °C), the morphology becomes equiaxed, and the surface turns to rough. A similar dendritic microstructure has also been reported for annealed Fe-Si-B alloys, and it has been suggested that the structure can be ascribed to rejection of B atoms and formation of Fe3Si phase (Zhang et al., 2006). It is known that exceeding a critical value for crystal size causes crystals to grow into dendrites, while dendrites cannot develop below that critical value (Mullins et al., 1963; Mullins et al., 1964). With regard to the crystallization morphology at lower or higher annealing temperatures, Kulik et al. (2006) have pointed out that higher

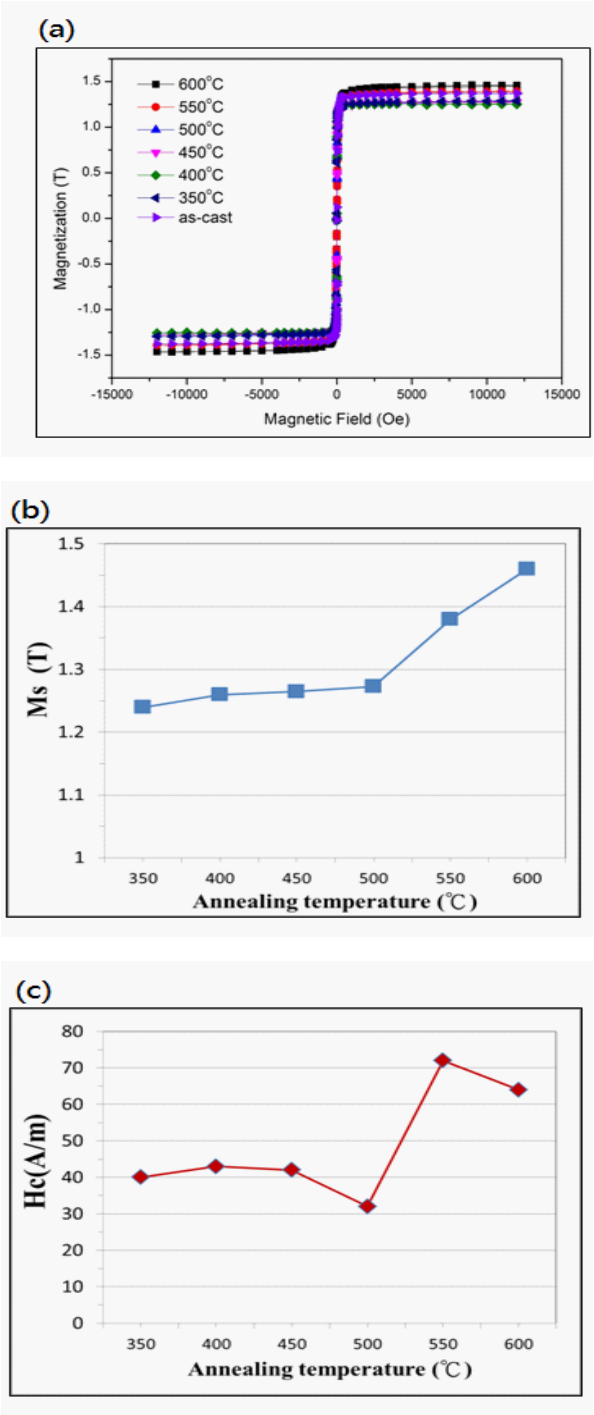

Figure 3. (a) Hysteresis loop of the $Fe_{74}Co_3Si_8B_{10}Al_1Nb_4$ alloy ribbons annealed at various temperatures for 10 min; (b,c) Saturation magnetization and coercive force of alloy ribbon as a function of annealing temperature. The saturation magnetization of $Fe_{74}Co_3Si_8B_{10}Al_1Nb_4$ alloy ribbons increase as the annealing temperature rises, while the coercive force decreases when the annealing temperature reaches 500 to 600 °C.

annealing temperatures lead to increased nucleation rate than in growth rate. During annealing at high temperature, the higher nucleation rate will result in finer crystal sizes, which cannot reach the critical value for dendrite formation.

The dependence of saturation magnetization (Ms) and coercive force (Hc) on annealing temperature of the $Fe_{74}Co_3Si_8B_{10}Al_1Nb_4$ alloy is shown in Fig. 3. Saturation magnetization (Ms) increases as annealing temperature rises up. For example, the minimum Ms, which is found at 350 °C, is 1.26 T. When the annealing temperature rises to 600 °C, the Ms also rises to 1.47 T. Since the α–Fe phase has stronger magnetocrystalline anisotropy and higher saturation magnetization than the amorphous phase, its precipitation will result in the saturation magnetization increasing with annealing temperature. The change of Hc with annealing temperature is more complicated than Ms, and it can be divided into three regions. In the annealing temperature range from 350 to 500 °C, the Hc decreases with rising the annealing temperature. This phenomenon is a result of structural relaxation by the gentle annealing treatment, which can effectively reduce the interior stress caused by the prior rapid cooling (Phan et al., 2006). The Hc increases rapidly as annealing temperature rises from 500 to 550 °C, implying a large degradation of the soft magnetic properties. The growing nanoparticles of the α–Fe phase in the amorphous matrix can considerably reduce the magnetic exchange coupling in the nanocrystalline material (Herzer et al., 1997). The Nb_3Si phase begins to precipitate in the amorphous matrix when the alloy is annealed at 550 to 600 °C. Because the Nb_3Si phase is a non-ferromagnetic material, it can effectively decrease the effective anisotropy and thus decrease the coercive force.

The variation of coercive force with annealing temperature of the present alloy ribbon can be divided into three stages as follows. Stage 1 (350~500 °C): the coercive force decreases with increasing annealing temperature due to structural relaxation; Stage 2 (500~550 °C): the growth of α–Fe phases in the amorphous matrix leads to increases in coercive force with annealing temperature; and Stage 3 (550~600 °C): the coercive force decreases with higher annealing temperature due to precipitation of Nb_3Si phase.

Conclusions

This investigation on the samples of $Fe_{74}Co_3Si_8B_{10}Al_1Nb_4$ alloy ribbons has yielded the following findings:

1. The alloy ribbon was amorphous, as determined by X-ray diffraction.
2. Based on the Kissinger equation, it was found that the activation crystallization energy of $Fe_{74}Co_3Si_8B_{10}Al_1Nb_4$ alloys was 490 KJ/mol which is higher than those of other iron-based amorphous alloys. The difference indicated that the thermal stability of the studied alloy system is superior to others.
3. Qualitative phase analysis from X-ray diffraction data identified a single phase of α–Fe in a sample annealed at 500 °C. The precipitates in alloy ribbons annealed at 600 °C were a mixture of FeB, Nb_3Si, and α–Fe phases.
4. The saturation magnetization of alloy ribbons increased from 1.26 T to 1.47 T when the annealing temperature rose from 350 to 600 °C, because more nanosized α–Fe particles precipitated in the amorphous matrix at higher annealing temperatures. In short, the amorphous matrix with lower magnetization can change magnetization property by appropriate annealing treatment.
5. The variation of coercive force with annealing temperature of the present alloy ribbon can be divided into three stages.

References

Ahmadi S, HR Shahverdi, and SS Saremi (2010) Kinetics of α-Fe nanocrystallization in Fe55Cr18Mo7B16C4 bulk amorphous alloy. Iranian Journal of Materials Science & Engineering 7: 25-29.

Borrego JM, JS Blázquez, SL-Pérez, JS Kim, CF Conde and A Conde (2014) Structural relaxation in Fe(Co)SiAlGaPCB amorphous alloys. J. Alloys Comp. 584: 607-610.

Chen SF, SH Huang, SJ Wang, SH Chen, and CC Chen (2014) Magnetic and Thermal Properties of Fe73.5Si13.5B9Cu1Nb3 Amorphous Ribbon and Ball-Milled Powders. Atlas Journal of Materials Science 1 (2): 38-43.

Cullity BD (2001) Elements of X-Ray Diffraction (3rd Edition).

Herzer G (1997) Handbook of Magnetic Materials, pp. 4-25.

Inoue A (2000) Stabilization of metallic supercooled liquid and bulk amorphous alloys. Acta Mater 48:279-306.

Inoue A, BL Shen and CT Chang (2004) Super-high strength of over 4000 MPa for Fe-based bulk glassy alloys in $[(Fe_{1-x}Co_x)_{0.75}B_{0.2}Si_{0.05}]_{96}Nb_4$ system. Acta Mater 52: 4093-4099.

Kulik T (2001) Nanocrystallization of metallic glasses. J. Non-Cryst. Solids 287: 145-161.

Mınguez P, HA Davies, I Todd, MRJ Gibbs, A Garcia-Arribas, and J Gutiérrez (2001) The magnetoelastic properties of as-quenched and annealed $Fe_{73.5-x}Al_xSi_{13.5}B_9Cu_1Mo_3$ (x=0,2,4,6) alloys. J. Non. Cryst. Solids 287: 428-431.

Mullins WW and RF Sekerka (1963) Morphological Stability of a Particle Growing by Diffusion or Heat Flow. J. Appl. Phys. 34: 323-328.

Mullins WW and RF Sekerka (1964) Stability of a Planar Interface During Solidification of a Dilute Binary Alloy. J. Appl. Phys. 35: 444-451.

Phan MH, HX Peng, MR Wisnom, YS Cho, and C Nguyen (2006) Effect of annealing on the microstructure and magnetic properties of Fe-based nanocomposite materials. Composites Part A: Applied Science and Manufacturing 37: 191-196.

Takeuchi A and A Inoue (2005) Classification of bulk metallic glasses by atomic size difference, heat of mixing and period of constituent elements and its application to characterization of the main alloying element. Mater Trans 46: 2817-2829.

Wang X, L Zhang, L Deng, J Xie and D Liang (2013) Structure, thermodynamic behavior and static magnetic properties of Al addition FeCoNbCuB alloy ribbons. J. Alloys Comp. 574: 112-118.

Yoshizawa Y, S Oguma and K Yamauchi (1998) New Fe-based soft magnetic alloys composed of ultrafine grain structure. J. Appl. Phys. 64: 6044-6046.

Zhang YR and RV Ramanujan (2006) Microstructural observations of the crystallization of amorphous Fe–Si–B based magnetic alloys. Thin Solid Films 505: 97–102.

Zuo B, T Sritharan, YB Teo, and M Damayanti (2005) Effects of ternary alloying on mechano-synthesis and nano-crystal stability of an iron-silicon alloy. J. Alloys Comp. 390: 82-87.